Effect of Fumed Silica and Draw Ratio on Nanocomposite Polypropylene Fibers

Luca Fambri [1,2]*, Izabela Dabrowska [1], Riccardo Ceccato [1,2] and Alessandro Pegoretti [1,2]

[1] Department of Industrial Engineering, University of Trento, via Sommarive 9, 38123 Trento (Italy); E-Mails: izabela_dabrowska84@wp.pl (I.D.); riccardo.ceccato@unitn.it (R.C.); alessandro.pegoretti@unitn.it (A.P.);

[2] National Interuniversity Consortium for Science and Technology of Materials (INSTM), Via G. Giusti 9, 50121 Firenze, Italy;

* Author to whom correspondence should be addressed; E-Mail: luca.fambri@unitn.it (L.F.); Tel.: +39-0461-282413; Fax: +39-0461-281977.

Abstract: Hydrophylic fumed silica AR974 was tested as a potential nanofiller for the production of composite isotactic polypropylene filaments/fibers (containing 0.25-2% vol of nanoparticles) via melt compounding and subsequent hot drawing. The objectives of this study were following: (i) to investigate the effects of the composition and of the processing conditions on the microstructure and the thermal and mechanical properties of the produced fibers; (ii) to separate the effects of silica addition from those produced by fiber drawing; (iii) to interpret the changes in the matrix molecular mobility (produced by silica and/or drawing).

SEM microscopy evidenced a good dispersion of nanoparticles at fractions up to 0.5% of the nanofiller. XRD analyses revealed the increase in crystallinity after drawing of both neat PP and produced nanocomposite fibers. Consequently, tensile modulus and strength of the fibers were enhanced. Drawn fibers containing 0.25-0.5% of nanofiller showed also a remarkable increase in the creep resistance. Loss modulus of drawn fibers showed a pronounced α-relaxation peak at about 65°C; the higher the draw ratio, the higher the peak intensity. In general, the thermal and mechanical properties of composite fibers were improved due to the combined effects of nanofiller reinforcement and fiber orientation produced during hot drawing.

Keywords: fumed silica; fibers; drawing; polypropylene; XRD; nanocomposites, draw ratio

1. Introduction

”Fiber” is defined as “a unit of matter characterized by flexibility, fineness and high ratio of length to thickness” [1]. For successful application of fibers, market requirements encompass adequate mechanical, chemical and thermal stability. In particular, fibers have found applications in clothing and furnishing, but they are also widely used in various industrial sectors such as insulation, composites, geotextiles and filtration. The fibers traditionally used for textile applications such as clothing, household goods and some technical products are made of semi-crystalline linear polymers, due to their possibility to be molecularly oriented during processing. Most industrially produced synthetic fibers belong to the one of the following four chemical types: polyamide, polyester, polyvinyl and polyolefin [2]. On the market volume basis, polypropylene fibers occupy the fourth position and are expected to rise by 5.8% p.a. until 2021 [3]. PP fibers have found many applications owing to their balanced physical and chemical properties, such as low density, high crystallinity, high stiffness or hardness, good chemical resistance of polymer [4, 5], and a relatively easy spinning which makes possible to achieve very high extension of macromolecular chains and their maximum alignment [6, 7]. The most common process for fiber productions consists of (i) the melt spinning in which fibers are extruded through a die and (ii) fiber drawing [8, 9]. Adjustments of extrusion temperature, die-size, winding speed and cooling temperature affect structure and properties of the as-spun fibers/filaments [10, 11]. Afterwards, as-spun fibers are subjected to a large and almost irreversible elongation (producing parallel orientation of chains), which accounts for enhanced mechanical properties. If the neck propagates during drawing over the entire sample and the as-spun fiber is extended uniformly until break, the achieved draw ratio is called the natural draw ratio [12].

In the last decades it has widely been proven that a small addition (< 5% wt.) of inorganic nanoparticles like silica [13-15], carbon nanotubes [16], layered silicates [17-19], silver and titania [20, 21] to polymeric matrices can profoundly improve physical properties of produced fibers, e.g. mechanical properties, gas barrier properties, fire retardance, antibacterial properties [14, 17, 20-27]. Silica has been largely used for improving PP properties, as documented by various papers dedicated to nanocomposite compounding by using either internal mixer [27-31] or melt extrusion [30-32], followed by injection molding or compression molding for characterization of bulk specimens. In order to improve the interaction between polypropylene and silica either addition of compatibilizer, mainly maleic anhydride grafted polypropylene PP-g-MA, [28, 31, 33, 34] or silica functionalization [25, 35, 36] have been reported in literature, showing the effects in dependence on the type of polypropylene (homopolymer, copolymer, or blend), percentage of compatibilizer, filler content, and compounding process.

In our previous paper, we have described the production of nanocomposite PP fibers containing fumed silica Aerosil®R805, i.e. a hydrophobic silica treated with octylsilane, and we have indicated optimum improvements in mechanical properties at the filler fraction 0.5% by vol. [15]. Following those previous results, the aim of the present work is to shed more light on the distinct effects of nanosilica content and of fiber drawing on the fiber properties. At this purpose, a different type of silica, i.e. hydrophobic silica Aerosil®R974 modified with dimethyldichlorosilane, was selected for the formulation of nanocomposite and for the production and characterization of polypropylene melt spun fibers. Besides, this nanofiller has higher specific surface area and higher bulk density then previously used [15] Aerosil®R805. Moreover, a commercial compatibilizer PP-g-MA was properly added to hydrophilic silica for evaluation of possible improvement of our PP/silica composites fibers. Our intention is the determination of key factors related to the processing conditions (nanofiller composition and draw ratio) in order to maximize the mechanical properties of fiber. Complementary information will be given by XRD analysis and dynamical mechanical measurements.

2. Materials and Mehods

2.1. Materials

Fumed silica (FS), polypropylene, and maleic anhydride grafted polypropylene were selected as nanofiller, matrix and compatibilizer, respectively.

Aerosil®R974, hydrophobic silica (surface treated with dimethyldichlorosilane) was kindly supplied by Evonik (Essen, Germany). Fumed silica nanoparticles are characterized by a specific surface area of 170 m^2/g, mean particle size of about 12 nm, and bulk density of 1.99 g/cm3 at 23°C. Before processing, fumed nanosilica powders were dried for 24h at 80°C in a vacuum oven.

Moplen HP500, isotactic polypropylene with density 0.905 g/cm3 at 23 °C and melt flow rate 1.8 g/10min at 230 °C and 2.16 kg, was received from Lati SpA (Vedano Olona, Italy) in the form of pellets.

Fusabond® P613, (PPgMA) maleic anhydride grafted polypropylene (maleic anhydride content = 0.25–0.50 wt%; melt flow rate 49 g/10 min at 190 °C and 1.0 kg; density 0.903g/cm3 at 23 °C), was supplied by DuPont™ de Nemours (Geneva, Switzerland). This compatibilizer was added to the composites with 0.5% of fumed silica, whereby the ratio PPgMA/FS was 1:1 or 2:1 by vol. (see Table 1).

2.2. Compounding, fiber spinning and drawing

Fibers were produced in a double step process (extrusion and hot-drawing) for compositions with 0.25 up to 2 vol% of fumed silica (Table 1). The compositions were selected in conformity with a preliminary study on compounding of AR974 with polypropylene followed by the characterization of nanocomposites plates produced by compression molding [37].

After compounding, the mixtures of PP and fumed silica were spun by a Thermo Haake PTW16 intermeshing co-rotating twin screw extruder (screw diameter 16 mm, L/D ratio 25, rod die diameter 1.65 mm) in order to produce fibers of about 500 µm diameter. The temperature profile from the hopper to the rod die was gradually increased in the range 130-230°C. As-spun fibers were fast cooled in water at room temperature and wrapped around a rotating cylinder (40mm diameter) rotating at 67rpm.

Draw ratio (DR) is defined according to the following equation in dependence on initial (S_i) and final (S_f) fiber section:

$$DR = \frac{S_i}{S_f} = (\frac{D_i}{D_f})^2 \tag{1}$$

where D_i and D_f are the initial and final diameters of the fiber. For instance, DR1 indicates as spun or undrawn fibers, whereas the fibers drawn ten times are indicated with DR10.

Fiber hot-drawing was performed in air at 145°C by using a hot-plate drawing apparatus 140 cm length (SSM-Giudici srl, Galbiate, LC, Italy) following the procedure described elsewhere [15]. Various drawn fibers were produced from a minimum draw ratio of DR4 up to a maximum value of about DR20, in dependence on the drawability of compounded nanocomposite.

The diameter of the fiber was measured on digital pictures taken by an optical microscope and analyzed by the image processing software (ImageJ®). The titer of fibers, T, or linear density, expressed in tex, is defined as the weight (in grams) of 1000 m of fiber following ASTM D681-07. It can be calculated from the fiber diameter according to eq. (2):

$$T = \frac{d\,\pi}{1000}\left(\frac{D}{2}\right)^2 \quad (2)$$

where d and D are the density and the diameter of the fiber, expressed in g/cm3 and micron, respectively. Nanocomposites were labeled with a code indicating the type of silica (AR974) and its volume percentage. For example, AR974-2 indicates a nanocomposite sample filled with 2 vol% of fumed silica Aerosil AR974. Neat polypropylene was designated as PP, and the samples of fibers containing maleic anhydride grafted polypropylene were labeled with the extended code PPgMA (see Table 1).

2.3. Characterization Techniques

Melt flow index (MFI) measurements were performed by a Dynisco LMI 400 plastometer according to ASTM D1238-10 at 230°C and 2.16Kg. About 3 grams of as spun fibers were cut and inserted into the cylinder, where were preheated for 5 min before extrusion. Melt flow was expressed as average values of five measurements.

Quasi-static tensile mechanical properties of fibers were performed at room temperature by using an Instron ®4502 tensile testing machine equipped with a load cell of 100 N. Single filaments with diameters 0.5 mm – 0.1 mm and gauge length of 30 mm were uniaxially tested at 50 mm/min up to break. According to ISO 527 standard, the elastic modulus was determined as a secant value between strain levels of 0.05% and 0.25%. Strain was evaluated by normalizing the cross-head displacement over the gauge length of the samples. At least five specimens were tested for each sample and the average values were calculated. Tenacity of fibers was calculated as the ratio between load at break and the titer.

Creep response of the fibers was tested by DMA Q800 dynamometer (TA Instruments) at 30°C. Both unfilled PP and PP-silica nanocomposite fibers with a gauge length of 10 mm were tested for 3600 s under a constant stress of 3 MPa, corresponding to about 10% of the stress at yield of as spun fiber [24]. The creep compliance D(t), computed as the ratio between the strain and the creep stress, was plotted against the logarithm of time. Appendix A-1 shows the best fitting parameters of Burgers model .

Thermogravimetric analysis (TGA) was performed in an air flow (25 mL/min) with fiber specimens of about 10 mg by using a TGA Q5000 IR (TA Instruments) equipment at a heating rate of 10 °C/min in the range 50-600 °C. The results in Table 4 represent the average of three tests. The rate of thermooxidation was evaluated at the maximum of the peak of derivative curve DTGA.

Scanning electron micrographs (SEM) were taken by a Philips XL30 environmental scanning electron microscope, at an acceleration voltage between 20 and 25 kV. Micrographs visualize the surface produced by fracturing the fiber specimens in liquid nitrogen.

X-ray diffraction (XRD) spectra were collected by using a Rigaku III D-Max diffractometer, in a θ - 2θ Bragg-Brentano geometry with a graphite monochromator in the diffracted beam (monochromatic radiation CuKα line with λ=1.54056 Å). The following parameters were adopted:

scan range: 3-40° in 2θ; sampling interval 0.05°; counting time: 5s, as previously set in the characterization of polyethylene – hydrotalcite nanocomposite fibers [38]. Fibers were tightly rolled up on an aluminum sample holder (~0.5 x 2 cm2) mounted orthogonal to the incident beam. As a rough approximation, the same areas of the samples were irradiated. Experimental spectra were handled in order to evaluate crystallographic features of the samples using a Jade 8® software (MDI – Materials Data, Livermore, CA, USA). Crystallinity, Xc, of the samples was calculated using the equation:

$$Xc = \frac{A_{cr}}{A_{cr}+A_{am}}100\ /\ f \quad (3)$$

where A_{cr} and A_{am} are the areas under the crystalline peaks and the amorphous halo, respectively, and f is the volume fraction of polymer matrix. Area values were calculated by a deconvolution step in the range 5°-30° of the diffraction spectra. Moreover, crystallite size dimensions for the more intense reflexes, L_{hkl}, were evaluated by means of the Scherrer equation [39]:

$$L = L_{hkl} = \frac{0.9\,\lambda}{\beta\cos\theta} \quad (4)$$

where λ is the monochromatic X-ray wavelength, θ is the incident angle of the radiation to the surface of the sample and β is the integral breadth at half maximum of the referred peak [40].

Dynamic mechanical thermal analysis (DMTA) was carried out with the DMA Q800 dynamometer (TA Instruments) in tensile mode in the temperature interval from -125 to 125°C with a heating rate of 3 °C/min by using a fiber clamp (gauge length of 10 mm; pre-stress of 0.01 N; sinusoidal strain with a frequency of 1 Hz and amplitude of 64 micron). Storage modulus and loss modulus of as spun and selected drawn fibers were measured and compared as function of temperature.

3. Results and Discussion

As spun fibers of neat and nanofilled polypropylene with or without compatibilizer are summarized in Table 1. Melt flow analysis was performed in order to evaluate the effect of twin-screw extrusion on polymer matrix and on compounded nanocomposites. Subsequently fiber were drawn at different draw ratio and characterized as described and discussed in following paragraphs.

Table 1. Designation and composition of PP nanocomposites fibers.

Fiber	Fumed silica [vol.%]	PP [vol.%]	PPgMA [vol.%]	MFI [g/10min]
PP	0	100	0	1.84±0.08
AR974-0.25	0.25	99.75	0	2.04±0.10
AR974-0.5	0.5	99.50	0	2.40±0.14
AR974-1	1	99.0	0	2.52±0.08

AR974-2	2	98.0	0	2.69±0.20
AR974-0.5/C-0.5	0.5	99.0	0.5	3.20±0.15
AR974-0.5/C-1	0.5	98.5	1.0	3.62±0.20

3.1. Melt Flow Index of the prepared PP Composites

Table 1 evidences the melt flow index MFI after melt extrusion of various compositions. PP exhibits an almost constant value with respect to technical data sheet declared by the producer. On the other hand, the addition of fumed silica determined a slight increase of melt flow, that appeared directly proportional to the volume fraction of filler. A first interpretation is the attribution of experimental results to some thermal degradation of the PP matrix during processing, in analogy with the previous description of Dorigato after 15 mins of melt compounding [41]. However, in that case the increase of melt flow was attributed to the radical thermoxidation due to presence of oxygen in the chamber of internal mixer, and it was more markedly observed in neat polypropylene than in nanocomposite with fumed silica at 2% by vol. On the other hand, in the case of melt compounding in twin-screw extrusion described in this study, the amount of oxygen is certainly negligible, and the linear increase of melt flow of compounded nanocomposites could be attributed to the effect of organic layer of functionalized silica that could behave as internal lubricant, and consequently reduce the viscosity.

Moreover as expected, for the compositions with 0.5 and 1.0% of PP-g-MA, the significant increase of MFI can be ascribed to the higher MFI of the compatibilizer. Similar result was observed by Lee and Youn in polypropylene/layered-silicate nanocomposites, and it was considered as a negative effect, because it reduced the macromolecular orientation during melt spinning of fiber [42].

3.2. Tensile Mechanical Properties

Evaluation of mechanical properties is the crucial point in composites and fiber production. Both as spun and drawn fibers were extensively tested and compared as function of draw ratio (DR). The higher the drawing, the higher the fiber orientation, and the higher the modulus and the stress at break, and the lower the strain at break. Figure 1 show the relationship between tensile strength and the correspondent deformation at break for selected drawn fibers at different draw ratio. In particular, Figure 1 documents that the increase in stress at break is accompanied by decrease in the tensile strain at break as consequence of drawing. The latter quantity decreases with the draw ratio from about 1250% for as-spun PP to 34-32% for AR974-1 with DR15 (see also Table 2). Strain at break of as-spun fibers decreases with the fraction of incorporated fumed silica (Table 2), while after drawing process the difference between PP and nanofilled fibers diminishes so that the values achieved at the highest draw ratio DR15-DR20 are very similar.

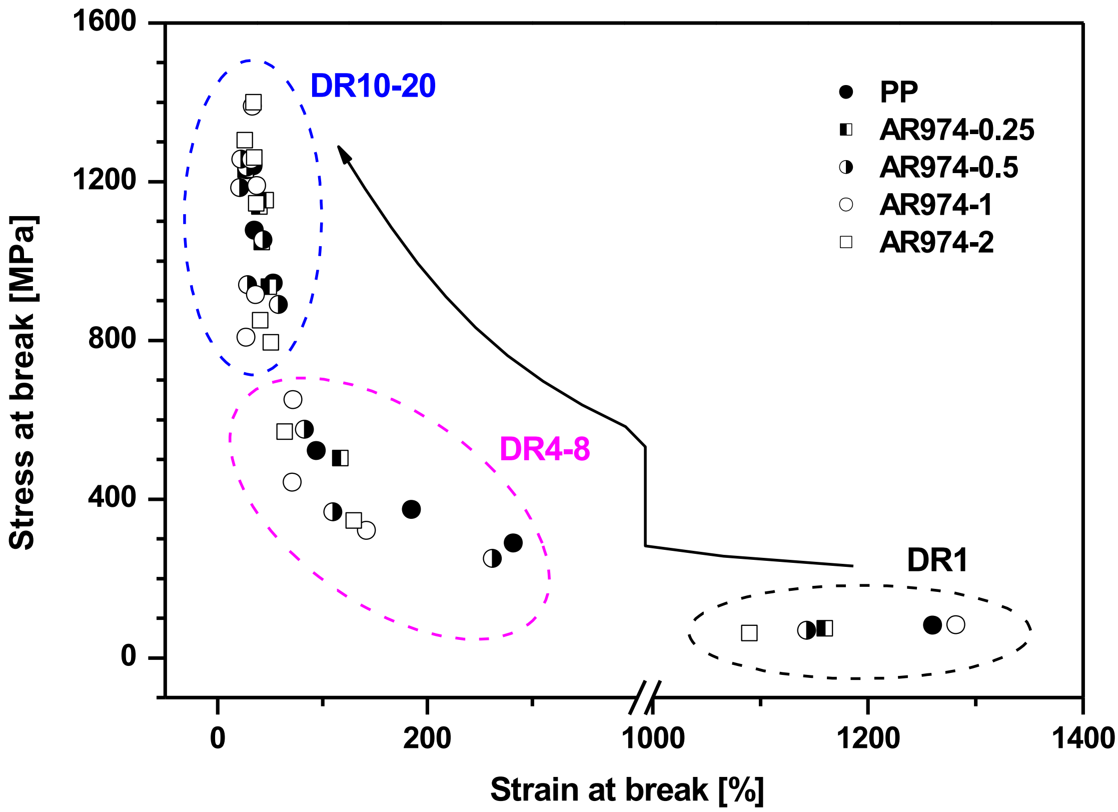

Figure 1. Representative comparison of stress at break as function of strain at break of selected neat and nanofiller PP fibers.

Table 2 compares titer, tenacity and other mechanical properties of selected fibers with or without compatibilizer; whereas the results of tensile modulus and strength of all drawn fibers without compatibilizer as shown in Figure 2 and 3, respectively. Tenacity of fibers is calculated as the ratio between load at break and the titer.

Two factors appeared of great relevance in nanocomposites fiber properties, i.e the filler content and the drawing ratio, that will be considered and discussed into details. Table 2 shows that the titer of the as-spun fibers varies from 174 tex of the neat matrix to about 179-186 tex of the nanocomposites, evidencing a direct dependence on the filler content, due the higher density of fumed silica. The titer decreases with rising DR. PP and nanocomposite fibers of about 35-37tex, 17tex and 11tex were produced via drawing to DR5, 10 and 15, respectively. Tenacity of as spun fiber was found to decrease with the filler content, whereas in drawn fibers some positive effects on tenacity were evidenced for composition up to 1% by vol of fumed silica. For instance, nanocomposite fibers AR974-0.25 and AR974-0.50 with DR10 show higher tenacity (116-127cN/tex) than corresponding PP fiber (104 cN/tex), while at DR15 both PP and nanocomposite fibers up to 1% of nanofiller have tenacity of about 136-137cN/tex.

Table 2. Titer, tenacity and other mechanical properties of neat and nanofilled PP fibers at selected draw ratios (DR).

Draw Ratio	Fiber	Titer* [tex]	Tenacity [cN/tex]	Diameter [µm]	Tensile modulus [GPa]	Stress at break [MPa]	Strain at break [%]
	PP	174.1	9.2	495±6	0.48±0.01	83±4	1260±15
	AR974-0.25	182.4	8.2	506±9	0.58±0.04	74±3	1160±45
	AR974-0.5	178.7	7.7	500±20	0.68±0.02	70±6	1144±54
DR1	AR974-1	179.7	9.1	500±8	0.65±0.01	83±6	1282±35
	AR974-2	186.3	6.7	506±9	0.67±0.02	62±8	1090±58
	AR974-0.5/C-0.5	180.8	7.7	503±4	0.60±0.02	70±6	1304±80
	AR974-0.5/C-1	183.7	7.7	507±8	0.66±0.04	70±2	1251±42
	PP	37.6	41.3	230±3	1.71±0.15	374±13	185±11
	AR974-0.25	37.7	55.4	230±4	2.45±0.11	503±16	117±5
	AR974-0.5	36.2	40.5	225±5	2.62±0.17	369±10	109±10
DR5	AR974-1	35.1	48.3	221±2	2.41±0.13	442±25	71±14
	AR974-2	36.8	37.3	225±4	1.81±016	346±17	129±13
	AR974-0.5/C-0.5	37.8	40.6	230±3	1.76±0.11	370±15	162±10
	AR974-0.5/C-1	35.5	53.3	223±1	2.44±0.17	485±20	96±15
	PP	17.7	104.3	158±3	5.30±0.15	944±25	53±5
	AR974-0.25	17.1	127.0	155±4	7.50±0.20	1153±30	46±2
	AR974-0.5	17.2	115.8	155±2	8.62±0.55	1054±45	43±6
DR10	AR974-1	17.3	99.9	155±4	5.70±0.45	915±45	36±12
	AR974-2	17.5	85.8	155±5	4.10±0.35	795±18	51±10
	AR974-0.5/C-0.5	17.2	107.2	155±1	5.80±0.30	976±20	33±13
	AR974-0.5/C-1	17.2	111.5	155±3	7.04±0.25	1015±35	35±10
	PP	11.6	137.0	128±2	7.88±0.35	1240±50	34±3
	AR974-0.25	11.3	135.5	126±2	8.30±0.50	1230±13	36±4
	AR974-0.5	11.3	135.9	126±4	9.41±0.25	1237±25	28±6
DR15	AR974-1	10.9	137.1	123±2	8.10±0.35	1256±50	32±8
	AR974-2	11.9	123.6	128±3	6.50±0.40	1145±38	37±5
	AR974-0.5/C-0.5	11.2	133.0	125±5	9.26±0.18	1211±20	30±7
	AR974-0.5/C-1**	11.5	119.7	127±3	9.05±0.20	1090±27	27±6

* for definition of Linear density and Tenacity see ASTM D861 *Standard Practice for Use of the Tex System to Designate Linear Density of Fibers, Yarn.*
**Fiber drawn at DR=12 (see Figure X).

Tensile modulus of nanofilled fibers increases with the percentage of fumed silica only up to 0.5% by vol. (Table 2). The highest values 8.3 GPa and 9.4 GPa at DR15 were achieved for AR974-0.25 and AR974-0.5 samples, respectively (7.9 GPa was found for PP fiber). The stiffening effect, especially at low nanofiller amount, could be attributed to (i) even distribution of nanofiller particles in the matrix and (ii) reduction of the mobility of macromolecules adhering to filler surface [25].

At elevated concentrations, nanofiller particles may form agglomerates (documented by the SEM and XRD analyses in the following paragraphs) that impair potential effects on increasing tenacity and strength, especially at higher DR.

It should be noted that existing literature evidences various dependencies of the stress at break of nanofilled PP fibers on filler fraction [14-17, 23-26, 43-46], i.e. either increasing, or insensitive, or even decreasing. Table 2 shows that stress at break of our samples is raised by fumed silica in the interval 0.25-0.5 vol.%, while slightly lower values were found for the fibers with 2 vol.% of filler.

To test the effect of the addition of PPgMA compatibilizer on mechanical properties of composite fibers, the optimum composition with 0.5 vol.% of fumed silica was selected. A stronger stiffening effect can be expected [43] due to (i) strengthened nanofiller/matrix interaction and (ii) more uniform nanofiller distribution in the polymer matrix. The obtained results (Table 2) show that addition of the compatibilizer (in the amounts of 0.5% and 1% vol) did not enhance the tensile modulus and stress at break of the nanocomposite fibers with 0.5 vol. % of the fumed silica. It worth noticing that at low draw ratios the strain at break of composites containing the compatibilizer is slightly higher than AR974-0.5 without compatibilizer. However, for DR10-15 the difference becomes less significant and at the highest DR is virtually negligible. Moreover the effect of compatibilizer (C) addition to polypropylene on tensile modulus and strength is shown in Figure 2.

a)

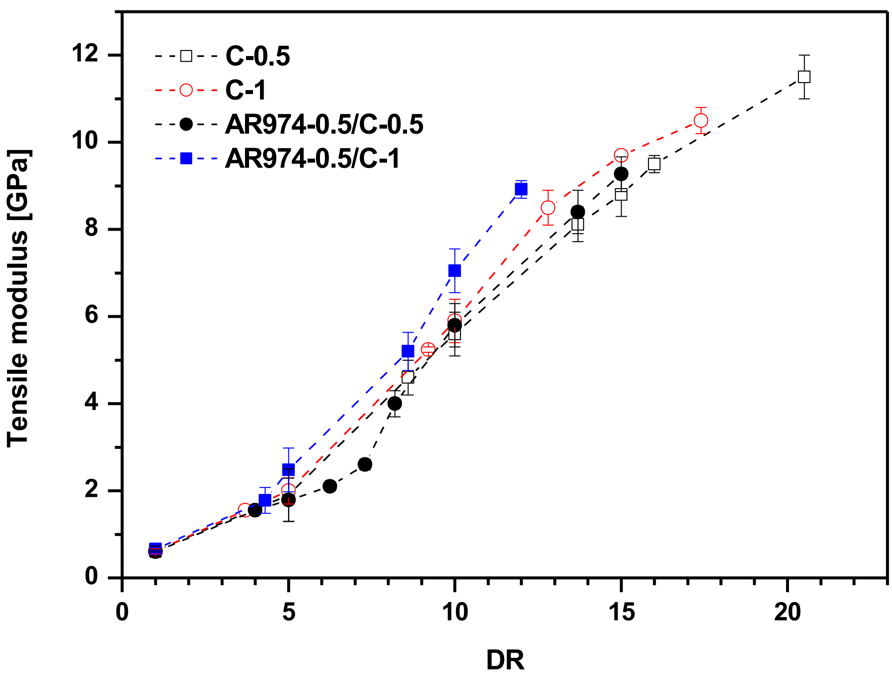

b)

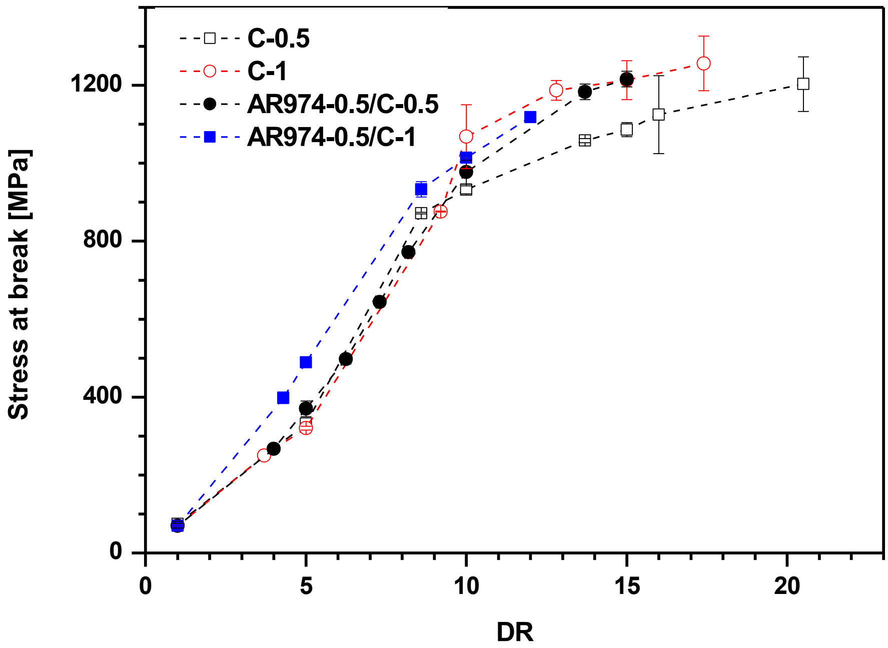

Figure 2. Effect of PP-g-MA on tensile modulus (a) and tensile strength (b) of PP fibers at with different content of compatibilizer (C), 0.5% and 1%, with and without 0.5% of fumed silica (percentage by volume).

Both draw ratio and filler content can affect the properties of the fiber. In general, the higher the draw ratio, the higher the modulus, the higher the strength, and the lower the strain at break of the fiber. Morover, the higher filler content, the higher the modulus of composite materials. However, in the case of fiber nanocomposite, the modulus of drawn fiber is not always increased with the filler content (Table 2), because the combined effects of material composition (filler content) and processing conditions (compounding and especially drawing) are not directly cooperative.

Various approaches could be considered and various parameters have been calculated from tensile mechanical properties, according to Equations 5-11, and summarized in Table 3.

Relative tenacity at constant draw ratio (RT_{DR}) is calculated as the ratio of the tenacity of nanocomposites (T_{AR974}) and the matrix tenacity (T_{PP}) for each set of drawn fibers, i.e.:

$$RT_{DR} = \frac{T_{AR974}}{T_{PP}} \quad (5)$$

Relative tensile modulus at constant draw ratio (RTM_{DR}) calculated as the ratio of the modulus of nanocomposites (E_{AR974}) and the matrix modulus (E_{PP}) for each set of drawn fibers,, i.e.:

$$RTM_{DR} = \frac{E_{AR974}}{E_{PP}} \quad (6)$$

Relative tenacity referred to polypropylene (RT_{PP}) can be calculated as the ratio of the tenacity of nanocomposites (T_{AR974}) and the matrix tenacity (T_{PP}) at DR1, i.e.:

$$RT_{PP} = \frac{T_{AR974}}{T_{PP(DR1)}} \quad (7)$$

Relative tensile modulus referred to polypropylene (RTM_{PP}) calculated as the ratio of the modulus of nanocomposites (EAR974) and the matrix modulus (E_{PP}) at DR1, i.e.:

$$RTM_{PP} = \frac{E_{AR974}}{E_{PP(DR1)}} \quad (8)$$

Table 3. Relative tenacity and relative modulus at constant draw ratio or as function of undrawn PP fiber. Draw Stiffening Factor (DSF), Drawing Efficacy (DE) and Filler Efficiency (FE).

Draw Ratio	Fiber	Relative Tenacity RT_{DR} Eq. 5	RT_{PP} Eq.6	Relative Tensile Modulus RTM_{DR} Eq.7	RTM_{PP} Eq.8	DSF Eq.9	DE Eq.10	FE Eq.11
DR1	PP	1,00	1,00	1,00	1,00	1,00	1,00	//
	AR974-0.25	0,89	1,21	1,21	1,21	1,00	1,00	83
	AR974-0.5	0,84	1,42	1,42	1,42	1,00	1,00	83
	AR974-1	0,99	1,35	1,35	1,35	1,00	1,00	35
	AR974-2	0,73	1,40	1,39	1,40	1,00	1,00	20
DR5	PP	1,00	3,56	1	3,56	3,56	0,71	//
	AR974-0.25	1,34	5,10	1,43	5,10	4,22	0,84	173
	AR974-0.5	0,98	5,46	1,53	5,46	3,85	0,77	106
	AR974-1	1,17	5,02	1,41	5,02	3,71	0,74	41
	AR974-2	0,90	3,77	1,06	3,77	2,70	0,54	3
DR10	PP	1,00	11,04	1	11,04	11,04	1,10	//
	AR974-0.25	1,22	15,63	1,42	15,63	12,93	1,29	166
	AR974-0.5	1,11	17,96	1,63	17,96	12,68	1,27	125
	AR974-1	0,96	11,88	1,07	11,88	8,77	0,88	8
	AR974-2	0,82	8,54	0,77	8,54	6,12	0,61	-11
DR15	PP	1,00	16,42	1	16,42	16,42	1,09	//
	AR974-0.25	0,99	17,29	1,05	17,29	14,31	0,95	21
	AR974-0.5	0,99	19,60	1,20	19,60	13,84	0,92	39
	AR974-1	1,00	16,88	1,03	16,88	12,46	0,83	3
	AR974-2	0,90	13,54	0,82	13,54	9,70	0,65	-9

Draw Stiffening Factor (DSF_F) is calculated for each composition as the ratio of modulus of drawn fiber (E_{drawn}) as function of modulus of undrawn fiber (E_{DR1})

$$DSF_F = \frac{E_{drawn}}{E_{DR1}} \quad (10)$$

The efficacy of drawing (ED) for each composition is evaluated as the ratio between the draw stiffening factor DSF and the correspondent draw ratio

$$DE = \frac{DSF}{DR} \quad (11)$$

The efficacy of filler (EF) for each composition is evaluated from the difference of nanocomposite modulus (E) and the modulus of PP normalized to the volume fraction of the filler (f) and to the modulus of PP

$$\text{FE} = \frac{E_{NC} - E_{PP}}{f\ E_{PP}} \tag{11}$$

A comparative evaluation of the different parameters could be of relevant interest for discriminating the different effect of composition and processing. The stiffening effect can be visualized from the relative tenacity and the relative modulus at various draw ratio. For instance, the DSF and DE indicates the stiffening effect of 0.25% and 0.5% filler for DR10 and DR15, whereas some limitation in drawing could be deducted for nanocomposite fibers AR974-1 and AR974-2. The consistent effect of filler on fiber properties appears evident from the parameter FE for composition 0.25% and 0.5% of silica at all draw ratio, especially for DR10. From this findings, it is clear in general that for the production of nanofilled fibers the maximum draw ratio should be requested, but the filler content should be properly defined.

Another approach for evaluation of the draw ratio effect is shown in Figure 3 and 4, where tensile modulus and stress at break of high drawn fibers are reported as function of the inverse of draw ratio. In this way is easy to visualize in order the tendency of property improving not only as function of drawing, but also in dependence on the nanocomposite filler content.

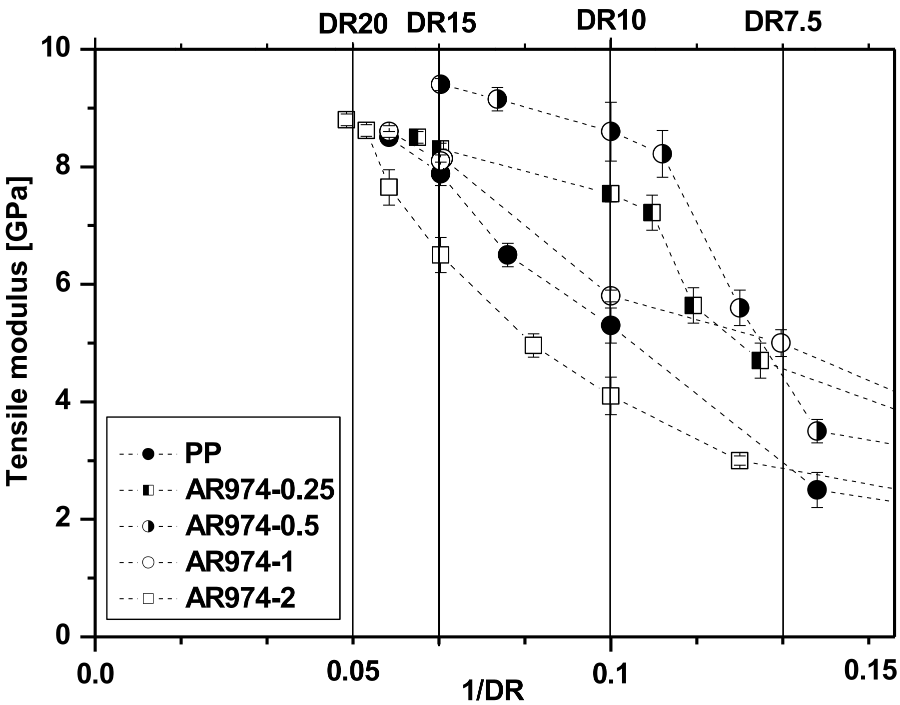

Figure 3. Tensile modulus of the neat and nanocomposite PP fibers with different amount of fumed silica as function of draw ratio (DR).

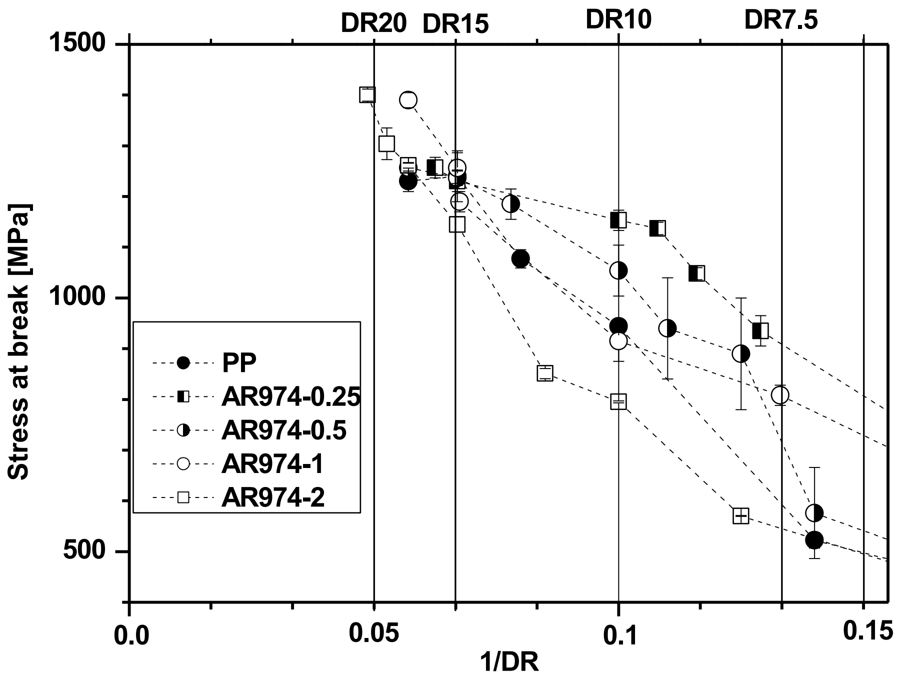

Figure 4. Stress at break of neat and nanofilled PP fibers with different amount of fumed silica as function of draw ratio (DR).

In particular the composition at low filler content (0.25% and 0.5%) seemed to show low modification at high draw ratio, whereas nanocomposite fibers with 1-2% of fumed silica showed further possibility of improving both tensile modulus and strength.

3.3. Short-term creep tests

Many practical applications of composite fibers encompass long-lasting applied loads, which make creep analysis and modeling inevitable [47]. In our simplified experiments, the strain of PP/fumed silica fibers was monitored as a function of time at a constant stress of 3 MPa applied for 3600 s. Creep compliance curves of neat and nanofilled fibers with different draw ratios are reported in Figures 5a and b. For as-spun fibers, the creep compliance of the fibers with 0.25-0.5 vol.% of nanofiller is higher by about 30-50% than that obtained for neat PP, while for the compositions with 1 and 2 vol.% no significant variation of creep compliance was observed.

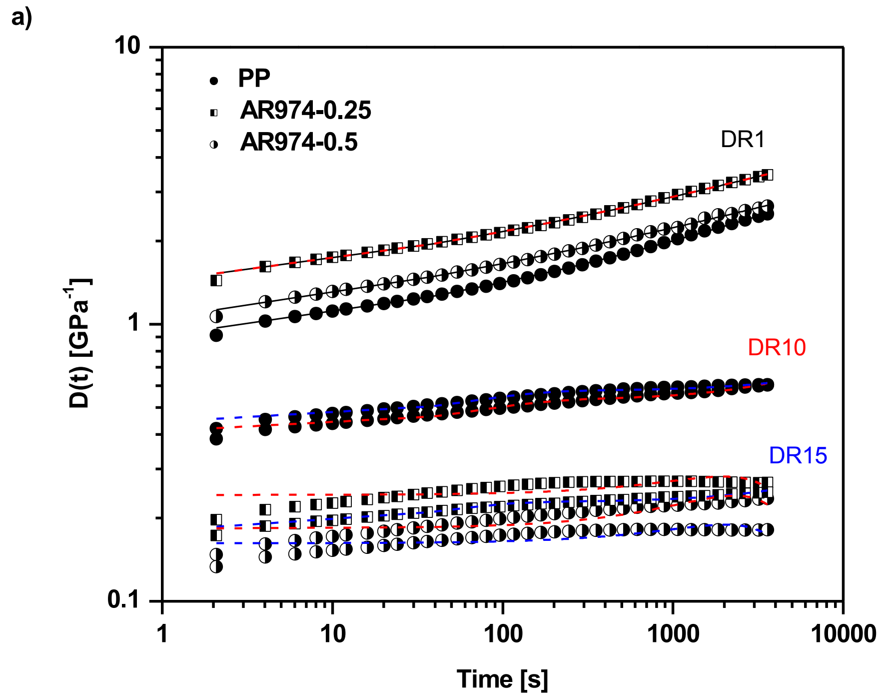

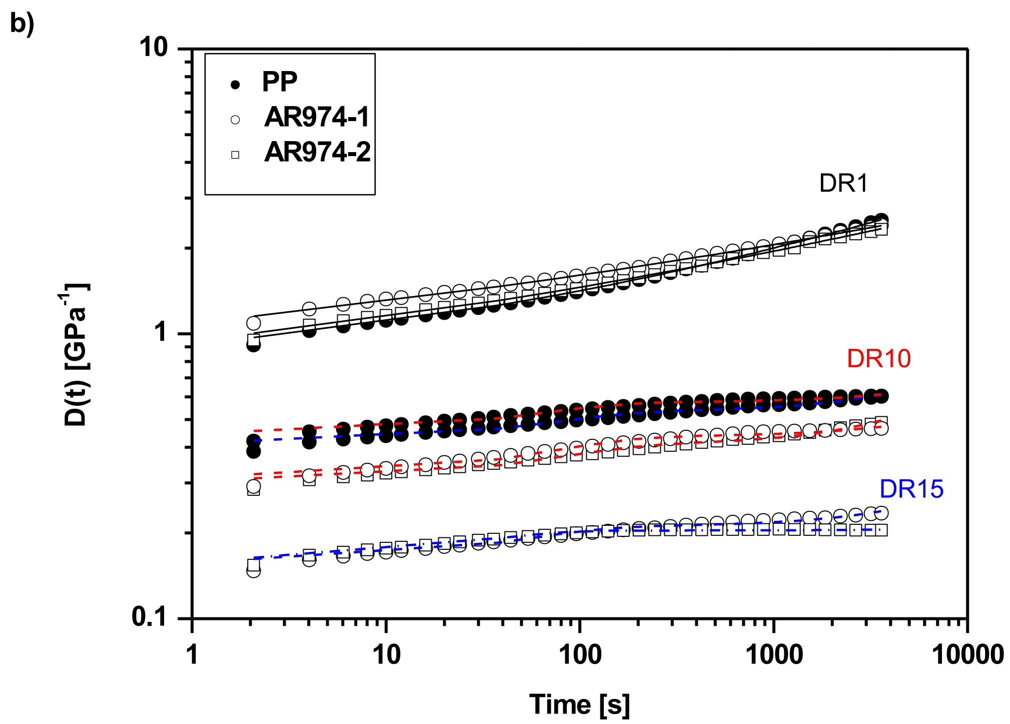

Figure 5. Tensile compliance of neat and nanocomposites PP fibers. Silica fraction: (**a**) 0.25 or 0.50 %; (**b**) 1 or 2 %. Draw ratios DR=1 (black line), DR=10 (red line), DR=15 (blue line). The fitting lines follow the Burgers model (see Appendix 1).

On the other hand, the incorporation of fumed silica contributes to remarkable reduction of the creep compliance of drawn specimens. The largest decrease in compliance is achieved for compositions with nanofiller fractions 0.25 and 0.5 vol.%, in agreement with tensile modulus (see Table 2). Similar results were reported for nanosilica composites [27, 48, 49] with HDPE matrix or PP matrix [50]. Lower creep compliance of the fibers with higher nanofiller fractions and DR15 might partly be related to a higher fraction of immobilized matrix entrapped in the agglomerates of nanofiller particles.

The creep resistance of nanocomposite fiber and it can be summarized as follows

AR974@DR1 ≤ PP @DR1 < PP @DR10/DR15 < AR974-1@DR10, AR974-2@DR10 <<
<<AR974-1@DR15, AR974-2@DR15 ≤ AR974-0.25@DR10/DR15 ≤ AR974-0.5 @DR10/DR15

3.4. Thermal Properties of Composite Fibers

Beneficial effect of fumed silica on the thermal degradation resistance of all composites (with respect to the neat PP) is documented by Figure 6.

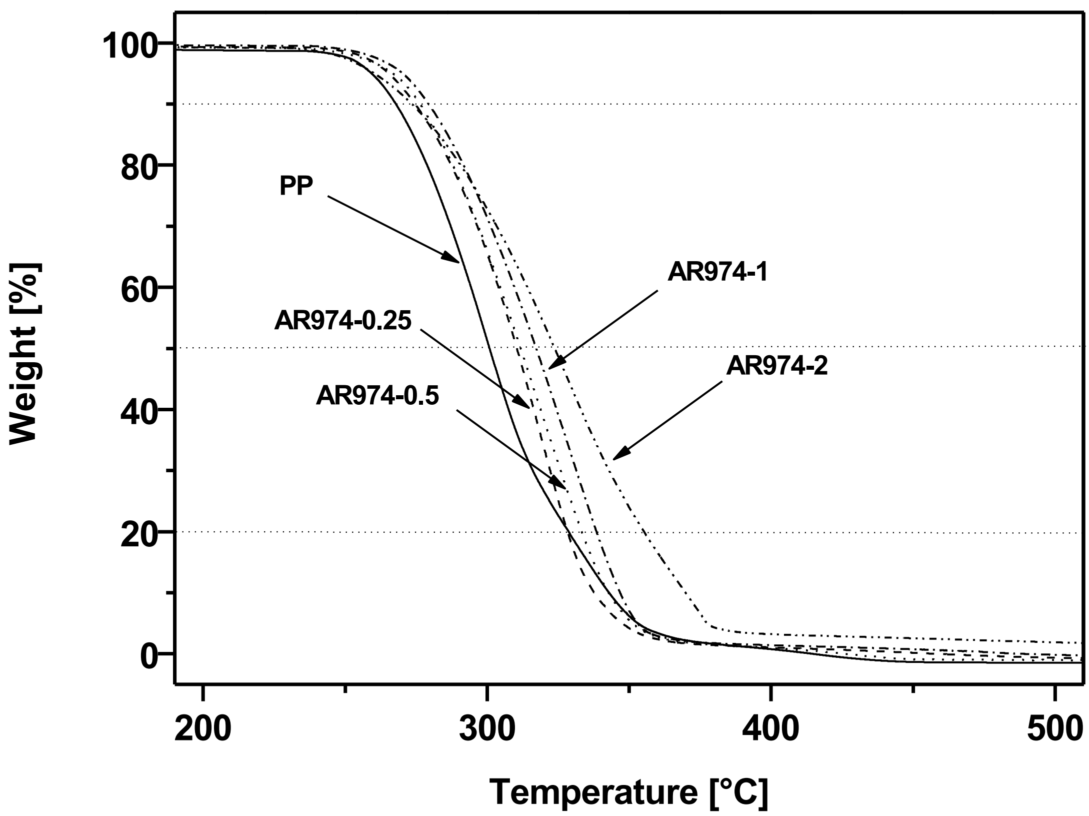

Figure 6. TGA thermograms of the neat PP and of the PP matrix in the as-spun fibers with various nanofiller fractions.

It is instructive to compare the thermal stability of the investigated materials at selected decomposition temperatures (Table 4). The temperatures $T_{0.1}$, $T_{0.5}$ and $T_{0.8}$ corresponding to the mass losses of 10%, 50% and 80% (for selected heating rate) of the PP-fumed silica fibers are higher than those of the neat PP, which confirms expected stabilizing effect of nanofiller particles under oxidizing atmosphere even at very low silica fractions. Analogous improvement has been reported for PP fibers containing fumed silica [14] or polyethylene plates with fumed silica or hydrotalcite [27, 40, 46].

Table 4. Selected TGA results of neat PP and nanofilled PP fibers.

Fiber	Temperature of selected mass loss - 10% $T_{0.1}$ [°C]	- 50% $T_{0.5}$ [°C]	- 80% $T_{0.8}$ [°C]	DTGA peak [°C]	Maximum degradation rate [-%/°C]	Residual mass at 600°C [%]
PP	267±2	301±3	328±2	299.7	-1.54	0.0±0.0
AR974-0.25	274±2	310±3	329±2	316.4	-1.43	0.5±0.1
AR974-0.5	276 ±3	312±3	333±2	318.8	-1.73	0.8±0.1
AR974-1	280±2	317±3	338±2	329.9	-1.44	1.2±0.3
AR974-2	274±2	324±2	355±3	328.3	-1.09	3.3±0.2

Improved thermooxidative stability, manifested by the shifts of $T_{0.1}$, $T_{0.5}$ and $T_{0.8}$ toward higher temperatures, can be ascribed to the barrier effect of the nanoparticles hampering the diffusion of the gaseous degradation products [51]. $T_{0.1}$ for the composite with 2 vol.% of AR974, which is slightly lower than the corresponding temperature of other PP-silica nanofibers, can tentatively be related to possible aggregate formation accounting for less effective barriers to diffusion. On the other hand, the effect of addition of 2 vol.% fumed silica is evident at higher degradation level (higher temperatures of decomposition $T_{0.5}$ and $T_{0.8}$) where silica nanoparticles create a temporary protection barrier. It is also worth noting that the peak of the derivative curve of TGA reveals the tendency not only to shift of the peak towards higher temperature, but also to reduce the maximum degradation rate, proportionally to the addition of fumed silica (see Table 4).

3.5. Microstructural Characterization

SEM images of as-spun nanocomposite fibers are reported in Figure 7a-e.

For low nanofiller contents of 0.25 vol.% and 0.5 vol.% (Figure 7 a and b), well dispersed silica nanoparticles are visible along with relatively small agglomerates of an average size in range of about 50-100 nm. As the silica fraction increases, larger agglomerates of the filler appear (Figure 7c and 2d). Agglomerates up to 500-800 nm can be observed for the filler fraction content of 2 vol.%,. These results are in conformity with previous research where similar sizes of nanosilica aggregates of particles were observed [22, 25, 34]. The aggregated morphology, observed for compositions with higher silica fractions, can be attributed to the strong interaction between the nanoparticles which becomes more and more important as the particle concentration increases [27].

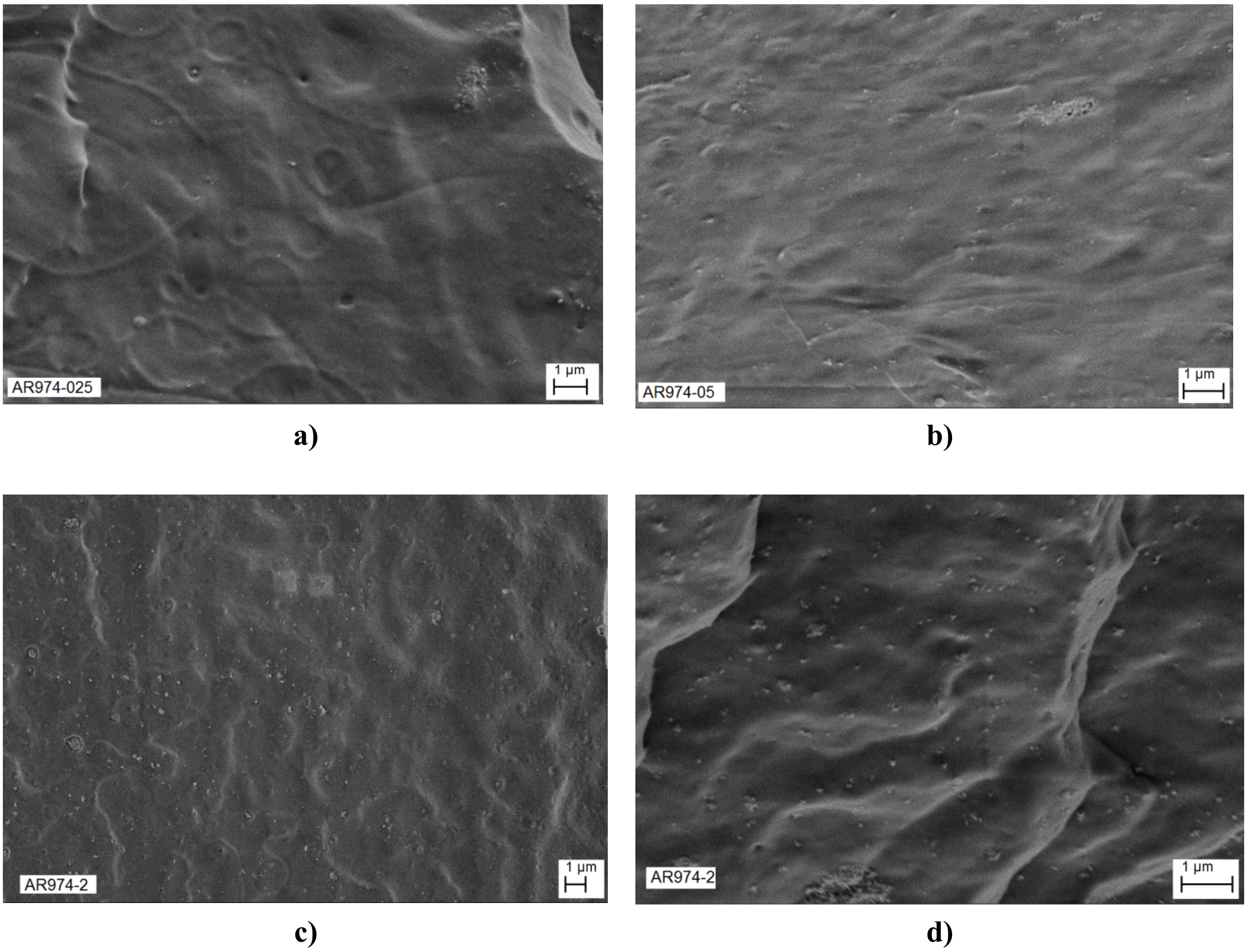

Figure 7. SEM images of cross section view of as-spun PP nanocomposite fibers with different nanosilica content 0.25 vol% (**a**); 0.5 vol% (**b**) and 2 vol%. (**c-d**).

3.6. XRD Analysis of the PP and Nanocomposite Fibers

XRD spectra of neat and nanofilled PP fibers are reported in Figure 8.As-spun PP fiber (DR=1) is characterized (Figure 8a) by two broad peaks centered at 2θ values of about 14.8° and 21° in 2θ [52-53]. They could be attributed to a mesomorphic form of isotactic PP characterized by not well-defined crystalline structures. Drawn fibers (DR10 or DR15) show well defined and more intense peaks. Incorporation of fumed silica into fibers (DR1) accounts for marked modifications of the observed XRD patterns (Figure 8b). Combined effects of silica fraction and drawing are visualized in Figure 3c. For the compositions with higher fractions of fumed silica (Figure 8b and 8c) XRD patterns clearly display - along with the broad peak centered at 21° - up to five distinct peaks at 2θ values of about 14°, 17°, 18.5°, 25.5° and 28°, which can be associated to an isotactic α-polypropylene crystalline phase (PDF n. 50-2397).

a)

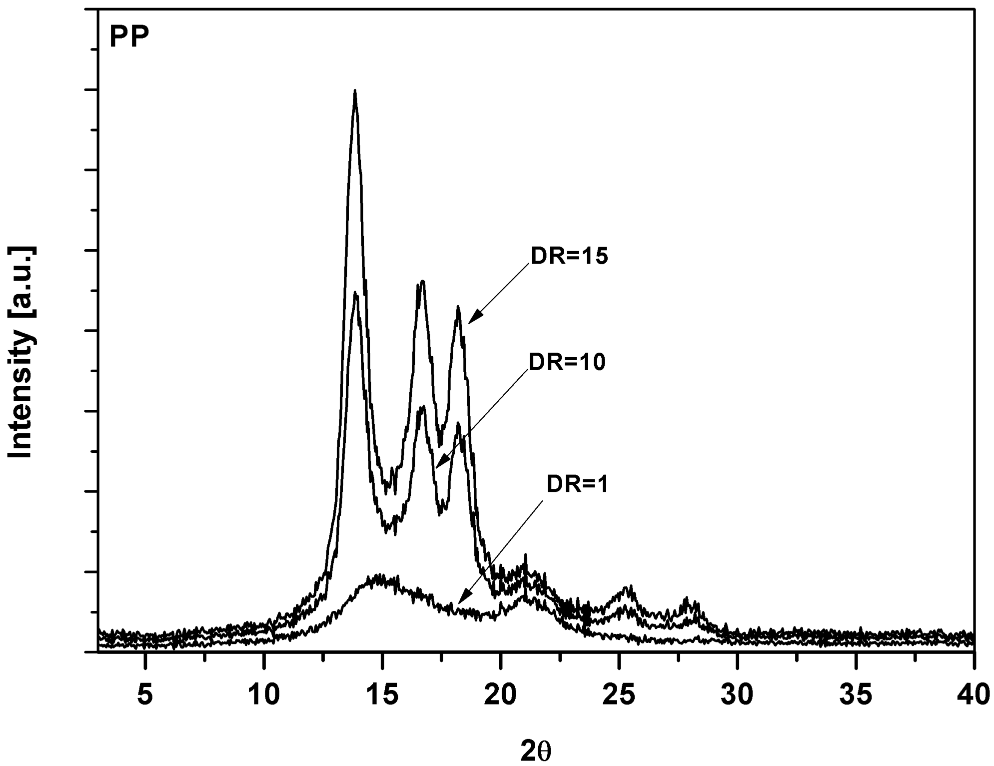

b)

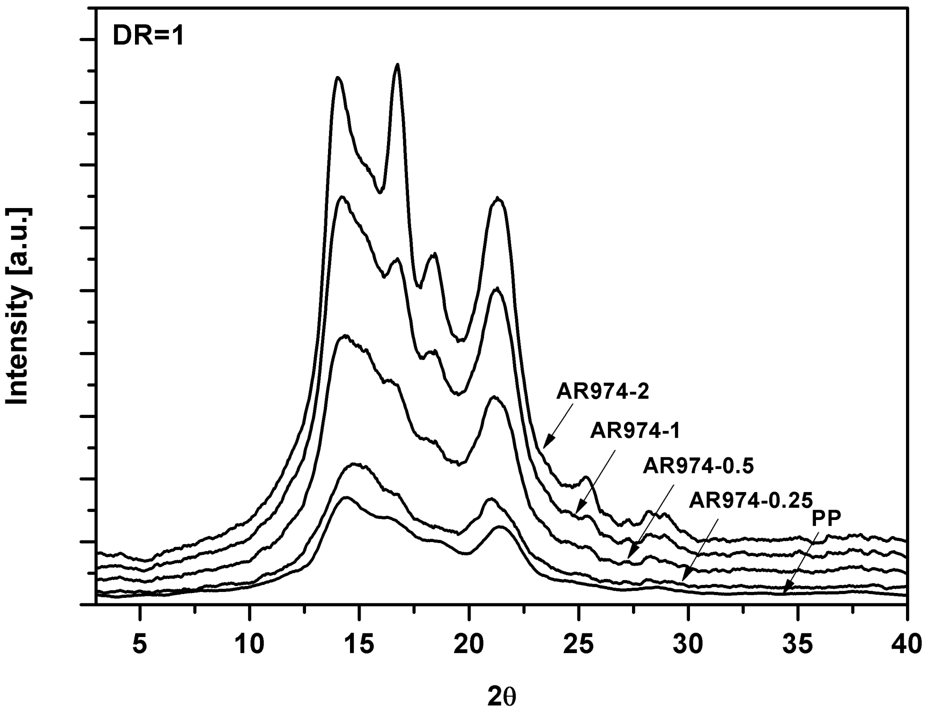

c)

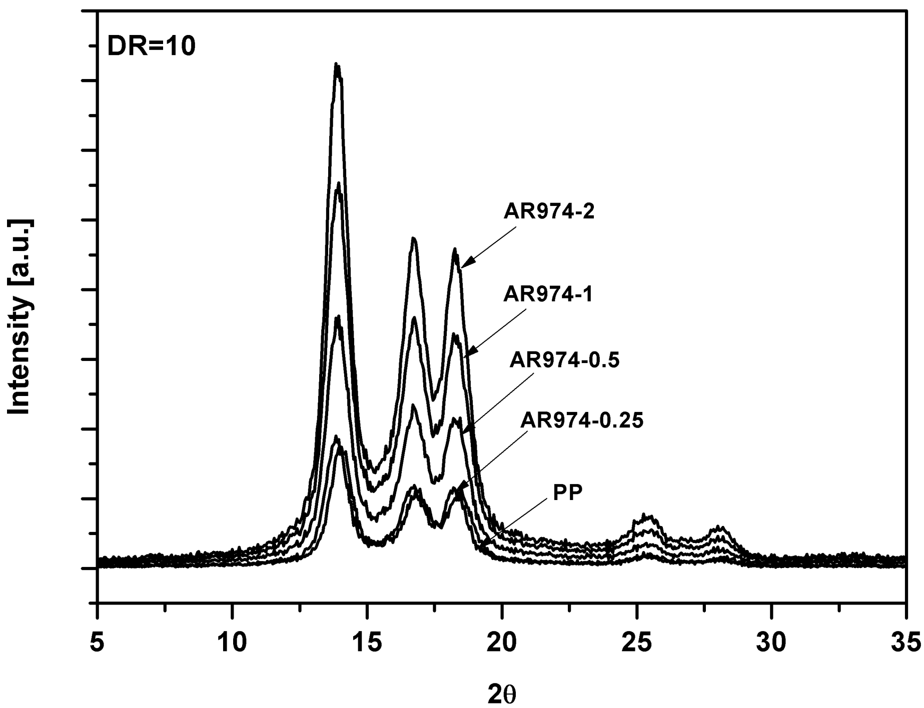

Figure 8. (**a**) Effect of draw ratio on XRD pattern of neat PP and effect of fumed silica content on XRD patterns of nanocomposite at (**b**) DR=1 and (**c**) DR=10.

Figure 8 reveals several important features: i) increasing of drawing leads to progressive increase in the peak of the α-crystalline phase and the reduction of the peak related to mesomorphic phase; ii) the previous peaks can be attributed to the corresponding reflexes, (110), (040), (130), (060) and (220), respectively; iii) comparing the experimental patterns with the standard phase of PP, it is noteworthy the absence of the (111) and (-131) reflexes of the α-phase, moreover, iv) an inversion between the relative intensities of (040) and (130) reflexes can be noticed, with respect to the above reported neat phase.

Crystallinity evaluated by a deconvolution process [40] of the amorphous and α-crystalline phases evidence that fumed silica leads to slightly higher crystallinity content: Xc = 24% for neat PP and about 28% for AR974-2 sample (Table 5).

Table 5. Crystallinity content and intensity ratio of the PP nanocomposite calculated from XRD measurements.

DR	Fiber	Xc [%]	I(040)/I(040)$_{ref}$	I(130)/I(130)$_{ref}$
	PP	23.6	1.0	1.0
	AR974-0.25	24.1	1.0	1.0
DR=1	AR974-0.5	23.5	1.0	1.1
	AR974-1	27.1	1.2	1.1
	AR974-2	27.6	1.7	1.1
	PP	57.7	3.1	4.1
	AR974-0.25	57.8	3.4	4.0
DR=10	AR974-0.5	48.1	3.1	3.9
	AR974-1	53.7	3.4	4.4
	AR974-2	56.4	3.1	4.6
	PP	55.7	2.1	2.6
	AR974-0.25	53.9	2.8	3.4
DR=15	AR974-0.5	52.4	3.1	3.3
	AR974-1	48.5	3.1	4.1
	AR974-2	50.0	2.5	3.1

Relative crystallinity fractions expressed in terms of the intensity ratios for a selected peak [54], is reported in Table 5. The ratio I(040) for each nanocomposite sample over I(040)ref for the as-spun (DR1) neat polypropylene fiber, set as reference material, Table 3 shows an increase of what for all compositions with silica fraction can be seen (Table 5). This allows us to conclude that fumed silica in polypropylene matrix may act as a nucleating agent [14,16]. A comparable trend is also observed for the I(130)/I(130)ref ratio, even if the drawing effect seems to be more important, as discussed in the following.

For as-spun material, the presence of two large peaks on a broadened ground suggests the coexistence of both the crystalline and amorphous phases. After drawing process, a new sharp peak appears which can be attributed to the development of α-crystal in PP [54, 55]. If the crystallinity percentage is compared, it is evident that (i) hot drawing, as usual in fiber orientation; (ii) the crystalline fraction increases from 24% for as-spun PP up to 58% for DR=10; (iii) with increasing DR up to 15 any further increase in crystallinity is not observed (Xc=56%). The same trends are observed for all studied PP nanofilled fibers. As summarized in Table 5, the highest values of crystallinity were obtained for fibers drawn to DR10, while at DR15 the crystallinity is somewhat lower.

The crystallite size estimated by means of the Scherrer equation from the data for the three more intense peaks of the α-phase (110), (040) and (130) reflections are summarized in Table 6.

Table 6. *Crystallite size dimensions (nm) of PP nanocomposite evaluated from XRD spectra.*

Fiber	Reflex (hkl)	DR=1	DR=10	DR=15
PP	(110)	3 (overlapped)	8.9±0.2	9.1±0.2
	(040)		8.7±0.4	7.7±0.4
	(130)		8.0±0.3	7.8±0.7
AR974-0.25	(110)	4.9±0.5	9.5±0.2	8.7±0.2
	(040)	3.0±0.7	8.8±0.4	8.6±0.4
	(130)	5.5±0.6	7.3±0.3	6.8±0.3
AR974-0.5	(110)	4.8±0.5	8.7±0.2	9.8±0.2
	(040)	3±1	8.5±0.4	9.2±0.5
	(130)	5.2±0.6	7.6±0.4	8.1±0.3
AR974-1	(110)	6.5±0.7	8.9±0.2	8.2±0.2
	(040)	3±1	8.0±0.4	6.3±0.4
	(130)	5.2±0.4	8.1±0.6	7.6±0.7
AR974-2	(110)	9.8±0.8	10.2±0.2	8.5±0.2
	(040)	12.7±0.6	9.8±0.4	8.0±0.7
	(130)	10±1	9.7±0.3	8.1±0.6

In the as-spun fibers, very small crystallites are found, but their dimensions rise with the drawing process (up to DR=10), which is in conformity with previous observations [56]. At draw ratio DR15, the tendency of a slight reduction of crystal size might be interpreted as a direct consequence of the decrease in crystallinity (see Table 5).

It can be concluded that the addition of the nanofiller leads to a more ordered structure as the detected peaks become sharper and more distinct (Figure 3b), thus confirming the presence of the α-crystalline phase of isotactic PP. This finding is a clear indication that fumed silica acts as a nucleating agent for the PP matrix. For the as-spun fibers (DR1), the nanofiller addition seems to play a key role because more crystallized structures can be obtained by increasing the silica nanoparticle content. This trend is documented by evaluated parameters, mainly intensity ratios and crystallite sizes (Table 6). Drawing process accounts for increase in the crystallite dimensions; on the other hand, the effect of nanofiller becomes less significant because the crystallization process is dominated by higher molecular orientation [57]. It can be concluded that the effect of nanofiller on fiber structure is more remarkable at low drawing ratios where the filler acts as a nucleating agent. With higher drawing ratios, the role of nanofiller is less significant because the crystallization process is dominated by molecular orientation during drawing [57].

2.7. DMTA Analysis

Dynamic mechanical thermal analysis has been used for evaluating the tensile storage E' and loss moduli E" of composite fibers (Figure 9). Generally, the interaction between nanoparticles and polymer matrix is expected to restrict the mobility of polymer segments adjacent to the particle surface. Consequently, the sub-glass transitions and the glass transition of the matrix may be shifted towards higher temperatures [45]. The effects of (i) silica fraction and (ii) DR on E' of composite fibers are summarized in Table 7. As can be seen, E' of the as-received (DR1) composite fibers only slightly rises with the silica fraction. On the other hand, E' of the composite fibers markedly rises with the drawing ratio up to DR15 (Figure 9), but the highest values of E' are reached for the compositions with the nanofiller fractions 0.25 and 0.5 vol.% (at DR10 and DR15).

a)

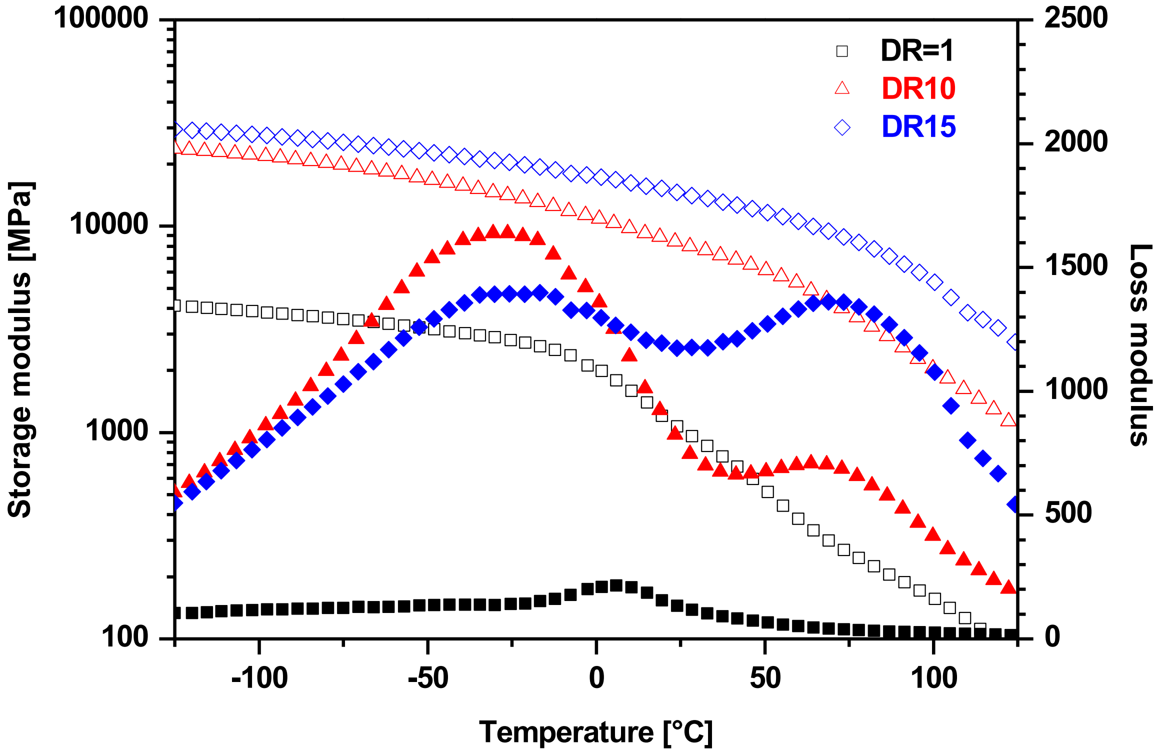

b)

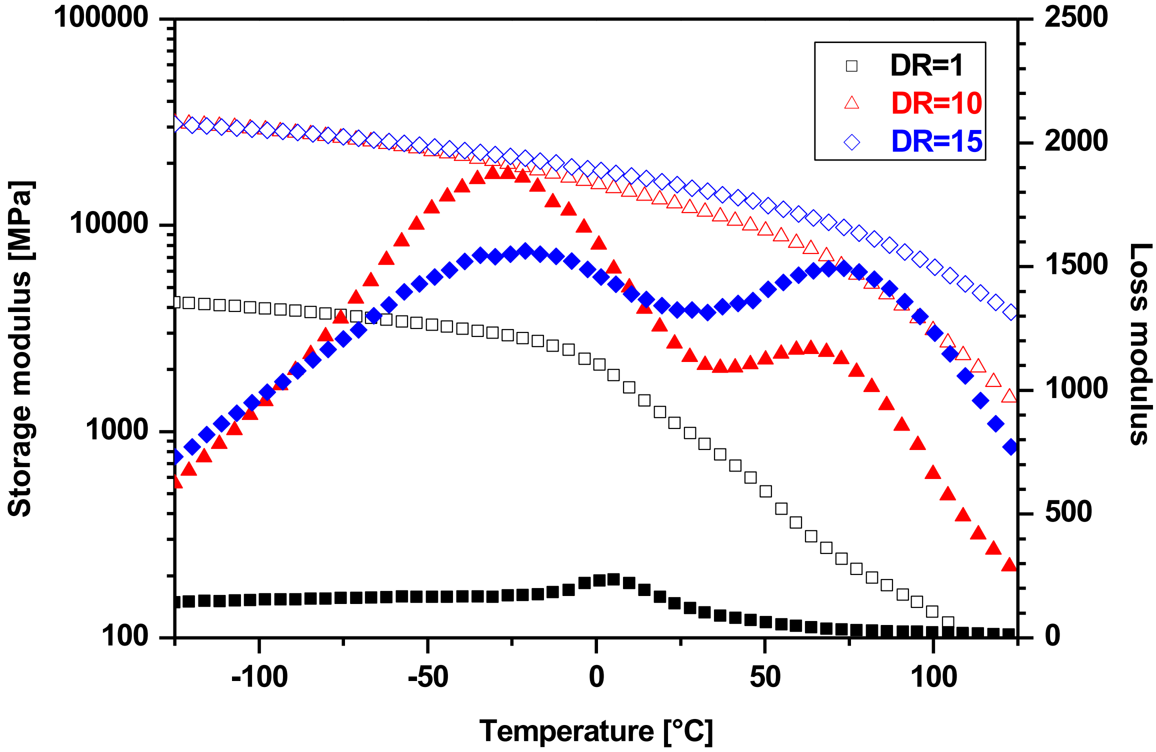
100000
10000
1000
100
Storage modulus [MPa]
2500
2000
1500
1000
500
0
Loss modulus
-100
-50
0
50
100
Temperature [°C]
DR=1
DR=10
DR=15

c)

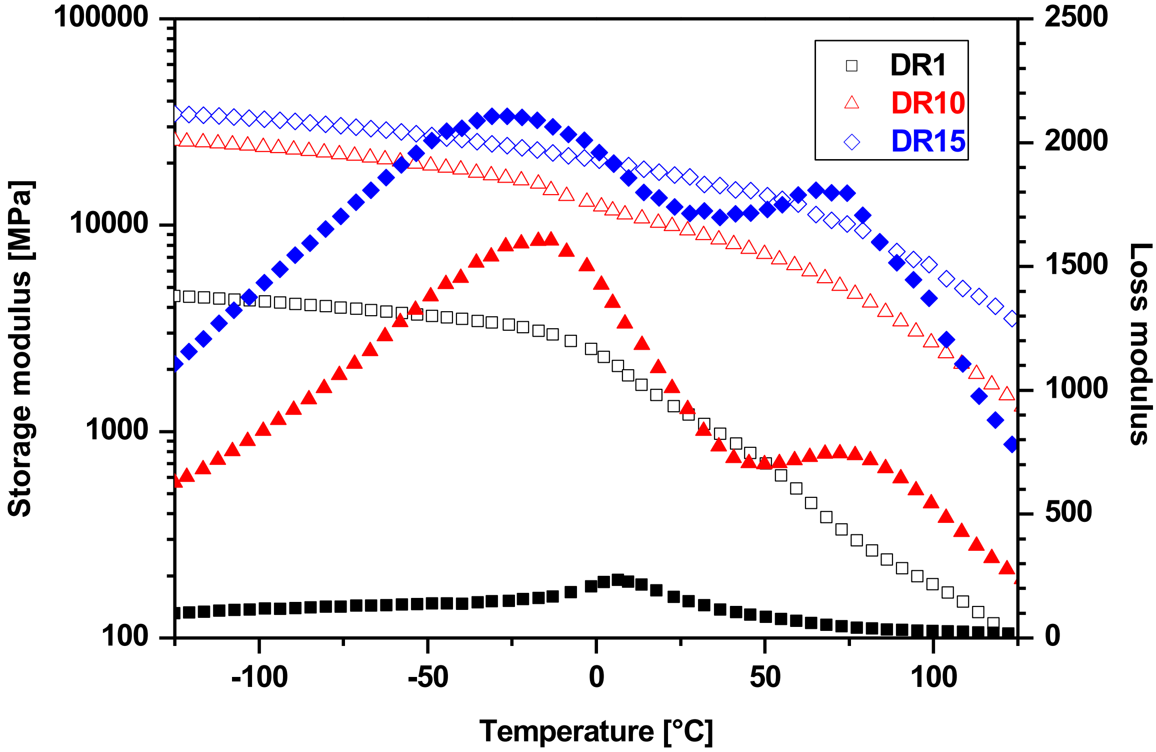
100000
10000
1000
100
Storage modulus [MPa]
2500
2000
1500
1000
500
0
Loss modulus
-100
-50
0
50
100
Temperature [°C]
DR1
DR10
DR15

Figure 9. Tensile storage modulus and loss modulus of neat and selected nanofilled PP fibers at various draw ratios. (**a**) PP; (**b**) AR974-0.5; and (**c**) AR974-1.

Table 8. Tensile storage modulus of neat and nanofilled PP fibers at selected temperatures for various draw ratios (DR).

DR	Material	Storage modulus at selected temperatures T [GPa]				
		T=-100°C	T=-50°C	T=0°C	T=50°C	T=100°C
DR=1	PP	3.86	3.22	2.10	0.50	0.15
	AR974-0.25	3.91	3.29	2.12	0.45	0.14
	AR974-0.5	4.01	3.36	2.15	0.52	0.13
	AR974-1	4.31	3.66	2.42	0.71	0.17
	AR974-2	5.04	4.21	2.49	0.80	0.28
DR=10	PP	22.02	16.72	10.85	6.24	2.06
	AR974-0.25	28.94	23.51	17.51	11.16	4.72
	AR974-0.5	29.47	22.98	15.91	9.43	3.10
	AR974-1	24.01	19.38	12.32	7.30	2.72
	AR974-2	19.88	15.00	8.86	4.64	1.66
DR=15	PP	27.74	22.70	17.33	11.68	5.34
	AR974-0.25	29.18	24.00	18.50	12.55	6.35
	AR974-0.5	32.51	27.04	20.80	14.32	6.78
	AR974-1	32.65	27.18	20.37	13.85	6.20
	AR974-2	28.17	23.28	16.90	12.12	5.91

Loss modulus E” dependences on temperature (Figure 9) reveal that neat PP for DR1 exhibits a small loss peak (generally designated as the β relaxation) located at about 5°C (Figure 9a), which corresponds to the glass transition of undrawn PP with mesomorphic morphology. Incorporation of 0.5 and 1 vol. % of nanosilica (Figure 9 b and c) to undrawn PP does not visibly affect the size and temperature location of the β peak, as shown in literature [34, 57]. In contrast, XRD patters show (Figure 8b) pronounced changes indicating partial transformation of the original mesomorphic form of PP into α-crystalline form. Therefore, it seems that DMTA analysis is not enough sensitive to indicate neither these morphological changes, nor possible immobilization of thin layers of the PP matrix adjacent to filler surface. On the other hand, XRD as well as DMTA patters are markedly affected by drawing procedure (Figures 8 and 9). PP specimens with DR10 and DR15 show two pronounced loss peaks: β peak at about -28°C and α peak at about 75°C. As can be seen, the α relaxation is related to DR, but it is not induced by the present nanofiller at DR1 (in other words, there is no indication of the presence of interphase layer with reduced molecular mobility in undrawn composite fibers). The intensity (the height of a loss peak) of the glass transition β peak of the neat PP markedly increases with DR, whereby T_β shifts to lower temperatures (Table A2 in Appendix 2), which is in conformity with our previous observation [15]. The α peak (or α relaxation [58]) observed at DR10 and DR15 (but not at DR1) is to be attributed to more hindered molecular motions, whose onset requires higher temperatures (energies) than the β motion in amorphous regions. It seems obvious that the α-relaxation is associated with limited molecular motions (hindered rotations) in the α-crystalline regions formed during drawing (as documented by Figure 8) . The intensity of the β and α relaxations of drawn fibers evidences their tendency to increase with the nanofiller fraction. The effect of the filler may be amplified proportionally to DR, because destruction of the filler aggregates (and increase of the contact area matrix/filler) by shear forces in the course of drawing is proportional todraw ratio.

We can attempt to better explain the shifts of T beta and T alpha induced by nanofiller fraction and/or drawing DR by correlating DMTA and XRD data (Figures 9 and 8). Neat PP at DR1 shows only one loss maximum – very much like amorphous polymers – which can be identified with glass transition of amorphous regions in the mesomorfic PP matrix (in this paper we will not consider the sub-glass transitions, if any). As can be seen, temperature location at about -5 C and the size of the β peak of PP are not perceptibly affected by incorporated silica. The α peak located at about 70°C is exclusively exhibited by drawn specimens, regardless the fraction of silica. Increasing DR accounts for decrease in T beta (from about 5°C to -25°C), while T alpha remains located around 74°C. XRD reveals (Figure 3) that drawing causes the transformation of the mesophase ("one-phase structure") of undrawn specimens into two separated phases, i.e. amorphous and α–crystalline phases. Temperature T beta = - 25°C of drawn specimens corresponds to standard Tg given for isotactic PP.

Figure 9 also shows that for the neat PP and composite with 0.5 % of silica the height of the α loss maximum rises when DR rise from 10 to 15, which is accompanied by reduction of the β loss maximum (temperature dependences of E" are crossing at about 10°C). This "transformation" of the loss peaks is the manifestation of the increasing fraction of the α–crystalline phase (due to drawing) and, consequently, of the decreasing fraction of amorphous phase.

Table A2 in Appendix 2 evidences that the α-loss peak rises with nanoparticle fraction and draw ratio. Besides, a shift towards higher temperatures can be seen, i.e. from 67-69°C for neat PP up to 73-76°C for fibers of AR974-1 drawn to DR10 and for fibers of AR974-2 drawn to DR15. These data indicate that the drawing process accounts for improving the dispersion of the nanoparticles in the matrix and formation of a more compact arrangement of chain segments.

Sumita model (see Appendix A-2) was applied to tentatively evaluate the effective volume fraction of the immobilized phase adjacent to filler surface by using data on loss modulus peak. The relative maximum matrix fraction immobilized on the filler surface was observed for 0.25 and 1.0% vol. of nanofiller, suggesting a good dispersion of nanosilica in draw fibers.

4. Conclusions

Production of nanocomposite fibers/filaments consisting of isotactic polypropylene matrix and surface treated fumed silica AR974 was realized via the double step process consisting of melt extrusion and drawing. As spun fiber could be easily obtained after compounding by means of twin-screw extrusion for composition in between 0.25% and 2% by volume of nanofiller.

SEM microphotographs show that for low nanofiller contents (0.25 vol.% and 0.5 vol.%) well dispersed silica nanoparticles are visible along with relatively small agglomerates (average sizes in range of about 50-100 nm). The size of agglomerates in as spun fiber increases with the filler fraction and achieves 500-800 nm for 2 vol.% of the filler.

XRD analysis of the PP crystallinity evidences that fumed silica induces formation a slightly higher crystalline fraction: Xc = 24% for neat PP, while about Xc = 28% was found for the sample with 2% of AR974 silica. The increase of dimensions of crystallite size from about 3 nm determined for neat polypropylene, to about 5-12nm found for all nanocomposite compositions allows us to conclude that fumed silica in polypropylene matrix acts as a moderate nucleating agent.

As for the mechanical properties of nanofilled fibers, tensile modulus and tensile stress at break rose with (i) the silica fraction merely up to 1 vol. % and with (ii) increasing draw ratio of all samples throughout the DR interval tested. Various parameters have been proposed for the evaluation of drawing effect and the filler content.

Simplified tensile creep tests of as-spun fibers showed that the tensile compliance of the fibers with 0.25-0.5 vol.% of nanofiller is lower by about 30-50% than that of neat PP, while for the compositions with 1 and 2 vol.% no significant variation of creep compliance was observed. Analogous creep tests evidenced the reduction of creep compliance - with respect to the neat PP fibers - over the whole range of investigated draw ratios.

Also the storage modulus E' and loss modulus E" from the DMTA tensile tests confirmed the stiffening effect of fumed silica in PP composites. Similarly to static tensile tests, also E' was found to rise with the draw ratio of test fibers. A relative maximum at room temperature of E'=15.8 GPa was found for the composition with 0.5 vol.% of nanofiller and DR15. The maximum values E" of 2.1 GPa (beta-peak) and 1.8 GPa (alpha-peak) were achieved for 1.0 vol.% and DR15.

The incorporation of the nanofiller in the PP matrix also enhanced the thermal stability of composite fibers in comparison to neat PP as manifested by shifting the temperature of the maximum degradation rate from about 300°C to 330°C for composition with 1-2% of nanofiller.

The results confirm our previous data that polypropylene effectively reinforced with 0.25-2% of hydrophobic fumed silica surface modified either with octylsilane (AR805) or with dimethyldichlorosilane (AR974), can be easily spinned and also drawn into nanofilled fibers with tenacity up to 137cN/dtex.

Following melt flow analysis, the role of surface hydrophobic layer of modified silica could be further investigated for the possible role not only of internal lubricant, but also of high drawing promoter in nanocomposite fiber production.

Sumita model was applied to tentatively evaluate the effective volume fraction of the immobilized phase adjacent to filler surface by using data on loss modulus peak. The relative maximum matrix fraction immobilized on the filler surface was observed for 0.25 and 1.0% vol. of nanofiller, suggesting a good dispersion of nanosilica in draw fibers.

The compositions with 0.5 vol.% of fumed silica at various draw ratio, and with 1% vol at high draw ratio are found to be the most promising for low-cost improvements of mechanical properties and thermal resistance of produced fibers.

The authors wish to thank to Evonik (Essen, Germany) for donation the fumed silica Aerosil® R974 and to Lati SpA (Vedano Olona, Italy) for donation the polypropylene (Moplen HP500). The authors are very indebted to Professor Jan Kolarik for his assistance and valuable discussion.

Author Contributions

L.F. conceived and designed the experiments; I.D. performed the experiments; R.C. performed XRD analysis; I.D., A.P., R.C. and L.F. analyzed the data; I.D. A.P., R.C. and L.F wrote the paper.

Conflicts of Interest

The authors declare no conflict of interest.

References and Notes

1. Beech, S.R.; Farnfield, C.A.; Whorton, P.; Wilkins, J.A. *Textile Terms and Definitions*, 8th ed.; The Textile Institute: Manchester, UK, 1986.
2. Hearle, J.W.S. Fiber structure: its formation and relation to performance. In *Handbook of textile fiber structure*, Eichhorn, S.J.; Hearle, J.W.S.; Jaffe, M.; Kikutani, T., Eds.; Woodhead Publishing: Cambridge, UK, 2009; Volume 1 Fundamentals and manufactured polymer fibres, pp. 3-21.
3. Kutsch, O. *Market study: Polypropylene (3rd Edition)*. As viewed on line at http://www.ceresana.com/en/marketstudies/plastics/polypropylene/ (accessed on 29th July 2016).
4. Karacan, I. Structure-property relationship in polypropylene fibers. In *Polypropylene: An A-Z reference*, Karger-Kocsis, J., Ed.; Kluwer Academic Publishers: Dordrecht, The Netherlands, 1999; pp. 783-793.
5. Silva, L. P.; Barbosa, E. F. *Polypropylene: Synthesis, Applications and Environmental Concerns* (Polymer Science and Technology); Nova Science Publishers: New York, 2013.
6. Mather, R.R. The structure of polyolefin fibres. In *Handbook of textile fiber structure*, Eichhorn, S.J.; Hearle, J.W.S.; Jaffe, M.; Kikutani, T., Eds.; Woodhead Publishing: Cambridge, UK, 2009; Volume 1 Fundamentals and manufactured polymer fibres, pp 276-304.
7. Wang, I.C.; Dobb, M.G.; Tomka, J.G. Polypropylene fibres: Exploration of conditions resulting in high tenacity. *J. Text. Inst.* **1996**, 87, 1-12.
8. Gupta, V.B.; Mondal S. A.; Bhuvanesh Y. C. Spinning speed-throughput rate relationship for polyester, nylon, and polypropylene fibers. *J. Appl. Polym. Sci.* **1997**, 65, 1773-1788, DOI: 10.1002/(SICI)1097-4628(19970829)65:9<1773::AID-APP14>3.0.CO;2-O
9. Richaud, E.; Verdu, J.; Fayolle, B. Tensile properties of polypropylene fibers. In *Handbook of tensile properties of textile and technical fibres*, Bunsell, R. A., Ed.; Woodhead Publishing: Cambridge, UK, 2009; pp 315-331.

10. Tomka, J.G. Textile Fibres. In Comprehensive Polymer Science, Booth, C.; Price, C.; Allen, G.; Bevington, J.C., Eds.; Pergamon Press: Oxford, UK, 1988; Vol. 2 Polymer properties, pp. 487-510.
11. Ziabicki, A. Fundamentals of fibre formation. Wiley: London, UK, 1976.
12. Ward, I.M. Mechanical properties of solid polymers. 2nd ed.; Wiley: New York, 1983.
13. Rottstegge, J.; Zhang, X.; Zhou, Y.; Xu, D.; Han, C.C.; Wang, D. Polymer nanocomposite powders and melt spun fibers filled with silica nanoparticles. *J. Appl. Polym. Sc*i. **2007**, 103, 218-227, DOI: 10.1002/app.25162
14. Srisawat, N.; Nithitanakul M.; K., S. Characterizations of fibers produced from polypropylene/silica composite. *J. Mat. Min.* **2009**, 53-58.
15. Dabrowska, I.; Fambri, L.; Pegoretti, A.; Slouf, M.; Vackova, T.; Kolarik, J. Spinning, drawing and physical properties of polypropylene nanocomposite fibers with fumed nanosilica. *Exp. Pol. Lett.* **2015**, 9, 277-290, DOI: 10.3144/expresspolymlett.2015.25
16. Kumar, S.; Doshi, H.; Srinivasarao, M.; Park, J.O.; Schiraldi, D.A. Fibers from polypropylene/nano carbon fiber composites. *Polymer* **2002**, 43, 1701-1703.
17. Rangasamy, L., Shim, E., Pourdeyhimi, B. Structure and tensile properties of nanoclay–polypropylene fibers produced by melt spinning. *J. Appl. Polym. Sci.* **2011**, 121, 410-419, DOI: 10.1002/app.33619
18. Joshi, M.; Shaw, A.; Butola, B.S. Studies on composite filaments from nanoclay reinforced polypropylene. *Fib. and Pol.* **2004**, 5, 59-67.
19. Marcinčin A; Marcinčin K; Hricová M; Ujhelyiová A; Janicki J; Ślusarczyk. C. Structure, thermal and mechanical properties of PP/organoclay composite fibres. FIBRES & TEXTILES in Eastern Europe 2013, 21, 1(97) 18-23, Available online: http://www.fibtex.lodz.pl/article836.html (accessed on 28th July 2016)
20. Yeo S. Y., Jeong S. H. Preparation and characterization of polypropylene/silver nanocomposite fibers. *Polym. Int.* **2003**, 52, 1053–1057. DOI: 10.1002/pi.1215
21. Chiu C.-W., Lin C.-A., Hong P.-D. Melt-spinning and thermal stability behavior of TiO2 nanoparticle/polypropylene nanocomposite fibers. *J. Polym. Res.* **2011**, 18,367–372, DOI 10.1007/s10965-010-9426-0
22. Vladimirov, V.; Betchev, C.; Papageorgiou, A.V.; Bikiaris, G.D. Dynamic mechanical and morphological studies of isotactic polypropylene/fumed silica nanocomposites with enhanced gas barrier properties. *Compos. Sci. Technol.* **2006**, 66, 2935-2944, DOI:10.1016/j.compscitech.2006.02.010
23. Lorenzi, D.; Sartori, G.; Ferrara, G.; Fambri, L. Spinnability of nanofilled polypropylene. *Macromol. Symp.* **2011**, 301, 73-81, DOI: 10.1002/masy.201150310. Available online http://onlinelibrary.wiley.com/doi/10.1002/masy.201150310/full
24. Ruan, W.H.; Mai, Y.L.; Wang, X.H.; Rong, M.Z.; Zhang, M.Q. Effects of processing conditions on properties of nano-SiO2/polypropylene composites fabricated by pre-drawing technique. *Compos. Sci. Technol.* **2007**, 67, 2747-2756, DOI:10.1016/j.compscitech.2007.02.004
25. Wu, C.L.; Zhang, M.Q.; Rong, M.Z.; Friedrich, K. Tensile performance improvement of low nanoparticles filled-polypropylene composites. *Compos. Sci. Technol.* **2002**, 62, 1327-1340, PII: S0266-3538(02)00079-9

26. Rong, M.Z.; Zhang, M.Q.; Pan, S.L.; Friedrich, K. Interfacial effects in polypropylene–silica nanocomposites. J. Appl. Polym. Sci. 2004, 92, 1771-1781.
27. Dorigato, A.; D'Amato, M.; Pegoretti, A. Thermo-mechanical properties of high density polyethylene – fumed silica nanocomposites: effect of filler surface area and treatment. *J. Pol. Res*. **2012**. 19, 9889/1-9889/11, DOI 10.1007/s10965-012-9889-2
28. Palza, H.; Vergara, R.; Zapata P. Composites of polypropylene melt blended with synthesized silica nanoparticles. *Comp. Sci. Techn.* **2011**, 71, 535–540, DOI:10.1016/j.compscitech.2011.01.002
29. Grala, M.; Bartczak, Z.; Różański, A. Morphology, thermal and mechanical properties of polypropylene/SiO2 nanocomposites obtained by reactive blending. *J. Polym. Res.* **2016**, 23, 25, DOI 10.1007/s10965-015-0914-0
30. Pustak, A.; Denac, M.; Škapin, A.S.; Švab, I.; Musil, V.; Šmit, I. Mechanical and rheological properties of silica-reinforced polypropylene/m-EPR blends. *J. Polym. Res.* **2016**, 23, 163, DOI 10.1007/s10965-016-1062-x
31. Wu, C.L.; Zhang, M.Q.; Rong, M.Z.; Friedrich, K. Silica nanoparticles filled polypropylene: effects of particle surface treatment, matrix ductility and particle species on mechanical performance of the composites. *Compos. Sci. Technol.* **2005**, 65, 635-645. DOI:10.1016/j.compscitech.2004.09.004
32. Dong, Q.; Ding, Y.; Wen, B.; Wang, F.; Dong, H.; Zhang, S.; Wang, T.; Yang, M. Improvement of thermal stability of polypropylene using DOPO-immobilized silica nanoparticles. *Colloid Polym. Sci.* **2012**, 290, 1371–1380. DOI 10.1007/s00396-012-2631-0
33. Bouaziz, A.; Jaziri, M.; Dalmas, F.; Massardier, V. Nanocomposites of silica reinforced polypropylene: Correlation between morphology and properties. *Polym. Eng. Sci.*, **2014**, 54, 2187–2196, DOI 10.1002/pen.23768.
34. Bikiaris, D.N.; Vassiliou, A.; Pavlidou, E.; Karayannidis, G.P. Compatibilisation effect of PP-g-MA copolymer on iPP/SiO2 nanocomposites prepared by melt mixing. *Eur. Polym. J.* **2005**, 41, 1965-1978, DOI:10.1016/j.eurpolymj.2005.03.008
35. Srisawat, N.; Nithitanakul, M.; Srikulkit, K. Spinning of fibers from polypropylene/silica composite resins. *J. Comp. Mater.* **2012**, 46, 99-110, DOI: 10.1177/0021998311410477 http://jcm.sagepub.com/content/46/1/99.refs
36. Pustak, A.; Pucic, I.; Denac, M.; Švab, I.; Pohleven, J.; Musil, V.; Šmit, I. Morphology of polypropylene/silica nano- and microcomposites. *J. Appl. Polym. Sci*. **2013**, 128, 3099–3106, DOI: 10.1002/app.38487
37. Fambri, L.; Dabrowska, I.; Pegoretti, A.; Kolarik, J. Compounding of fumed silica and polypropylene. Production and characterization of nanocomposite plates. (Manuscript in preparation)
38. Fambri, L.; Dabrowska, I.; Pegoretti, A.; Ceccato, R. Melt spinning and drawing of polyethylene nanocomposite fibers with organically modified hydrotalcite. *J. Appl. Pol. Sci.* **2015**, 131 (10), DOI: 10.1002/app.40277
39. Scherrer, P. Bestimmung der Grösse und der inneren Struktur von Kolloidteilchen mittels Röntgensrahlen [Determination of the size and internal structure of colloidal particles using X-rays] *Nachr Ges Wiss Goettingen, Math-Phys Kl.* **1918**, 2, 98-100.

40. Papageorgiou, D.G.; Vourlias, G.; Bikiaris, D.N.; Chrissafis, K. Synergistic effect of functionalized silica nanoparticles and a β-nucleating agent for the improvement of the mechanical properties of a propylene/ethylene random copolymer. *Macromol. Mater. Eng*. **2014**, 299, 707-721, DOI: 10.1002/mame.201300320 http://onlinelibrary.wiley.com/doi/10.1002/mame.201300320/pdf
41. Dorigato, A.; Pegoretti, A. Reprocessing effects on polypropylene/silica nanocomposites. *J. Appl. Polym. Sci.* **2014**, 131, 40242, DOI: 10.1002/APP.40242
42. Lee, S.H., Youn, J.R. Properties of polypropylene/layered-silicate nanocomposites and melt-spun fibers. *J. Appl. Polym. Sci.* **2008**, 109, 1221-1231, DOI 10.1002/app.28222
43. Soitong Tawat, P.J. The relationship of crystallization behavior, mechanical properties, and morphology of polypropylene nanocomposite fibers. *J. Mater. Sci.* **2011**, 46, 1697-1704.
44. Joshi, M.; Viswanathan, V. High-performance filaments from compatibilized polypropylene/clay nanocomposites. *J. Appl. Polym. Sci.* **2006**, 102, 2164-2174.
45. Rong, M.Z.; Zhang, M.Q.; Pan, S.L.; Lehmann, B.; Friedrich, K. Analysis of the interfacial interactions in polypropylene/silica nanocomposites. *Polym. Int.* **2004**, 53, 176-183, DOI: 10.1002/pi.1307
46. Dabrowska I., Fambri L., Pegoretti A., Ferrara G. Organically modified hydrotalcite for compounding and spinning of polyethylene nanocomposites. *Express Polymer Letters*, **2013**, 7, 936–949, DOI: 10.3144/expresspolymlett.2013.91
47. Nielsen, L.E. Mechanical properties of polymers and composite. Marcel Dekker, New York 1974.
48. D'Amato, M.; Dorigato, A.; Fambri, L.; Pegoretti, A. High performance polyethylene nanocomposite fibers. *Exp. Pol. Lett.* **2012**, 6, 954-964.
49. Dorigato, A.; Pegoretti, A.; Kolarik, J. Nonlinear tensile creep of linear low density polyethylene/fumed silica nanocomposites: time-strain superposition and creep prediction. *Polym. Compos.* **2010**, 31, 1947-1955, DOI: 10.1002/pc.20993
50. Siengchin, S.; Karger-Kocsis, J. Creep behavior of polystyrene/fluorohectorite micro- and nanocomposites. *Macromol. Rapid Commun.* **2006**, 27, 2090-2094.
51. Vuorinen, E.; Nhlapo, N.; Mafa, T.; Karger-Kocsis, J. Thermooxidative degradation of LDPE nanocomposites: Effect of surface treatments of fumed silica and boehmite alumina. *Polym. Degrad. Stab*. **2013**, 98, 2297-2305.
52. Colombe, G.;, Gree, S.; Lhost, O.; Dupire, M.; Rosenthal, M.;Ivanov D. Correlation between mechanical properties and orientation of the crystalline and mesomorphic phases in isotactic polypropylene fibers. *Polymer* **2011**, 52, 5630-5643, DOI:10.1016/j.polymer.2011.09.035
53. Karacan, I.; Benli, H. The influence of annealing treatment on the molecular structure and the mechanical properties of psotactic polypropylene fibers. *J. Appl. Polym. Sci.* **2011**, 122, 3322–3338, DOI 10.1002/app.34440
54. Bhuiyan, M.K.H.; Rahman, M.M.; Mina, M.F.; Islam, M.R.; Gafur, M.A.; Begum, A. Crystalline morphology and properties of multi-walled carbon nanotube filled isotactic polypropylene nanocomposites: Influence of filler size and loading. *Composites Part A* **2013**, 52, 70-79.
55. Avci, H.; Kotek, R.; Toliver, B. Controlling of threadline dynamics via a novel method to develop ultra-high performance polypropylene filaments *Polym. Eng. Sci.* **2015** , 55, 327–339.

56. Avci, H.; Kotek, R.; Yoon J. Developing an ecologically friendly isothermal bath to obtain a new class high-tenacity and high-modulus polypropylene fibers, *J. Mater. Sci*. **2013**, 48, 7791–7804, DOI 10.1007/s10853-013-7427-1
57. Broda, J.; Gawlowski, A.; Slusarczyk, C.; Wlochowicz, A.; Fabia, J. The influence of additives on the structure of polypropylene fibres. *Dyes Pigm.* **2007**, 74, 508-511.
58. McCrum, N.G.; Ready, B.E.; G., W. Anelastic and dielectric effects in polymeric solids. Dover Publications: New York 1991, pp.378-383